

Unearthing a novel function of SRSF1 in binding and unfolding of RNA G-quadruplexes

Naiduwadura Ivon Upekala De Silva, Nathan Lehman, Talia Fargason, Trenton Paul, Zihan Zhang and Jun Zhang *

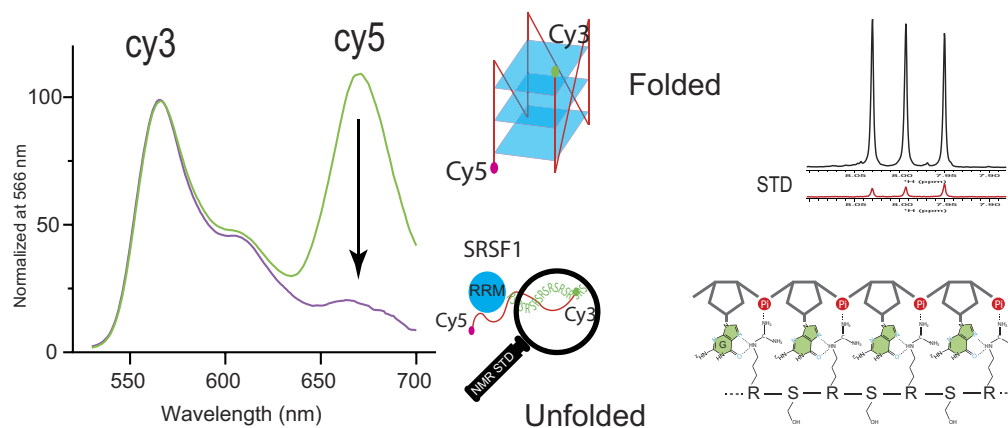
Department of Chemistry, College of Arts and Sciences, University of Alabama at Birmingham, CH266, 901 14th Street South, Birmingham, AL 35294-1240, USA

*To whom correspondence should be addressed. Tel: +1 205 934 2139; Fax: +1 205 934 2543; Email: zhanguab@uab.edu

Abstract

SRSF1 governs splicing of over 1500 mRNA transcripts. SRSF1 contains two RNA-recognition motifs (RRMs) and a C-terminal Arg/Ser-rich region (RS). It has been thought that SRSF1 RRM exclusively recognize single-stranded exonic splicing enhancers, while RS lacks RNA-binding specificity. With our success in solving the insolubility problem of SRSF1, we can explore the unknown RNA-binding landscape of SRSF1. We find that SRSF1 RS prefers purine over pyrimidine. Moreover, SRSF1 binds to the G-quadruplex (GQ) from the ARPC2 mRNA, with both RRM and RS being crucial. Our binding assays show that the traditional RNA-binding sites on the RRM tandem and the Arg in RS are responsible for GQ binding. Interestingly, our FRET and circular dichroism data reveal that SRSF1 unfolds the ARPC2 GQ, with RS leading unfolding and RRM aiding. Our saturation transfer difference NMR results discover that Arg residues in SRSF1 RS interact with the guanine base but not other nucleobases, underscoring the uniqueness of the Arg/guanine interaction. Our luciferase assays confirm that SRSF1 can alleviate the inhibitory effect of GQ on gene expression in the cell. Given the prevalence of RNA GQ and SR proteins, our findings unveil unexplored SR protein functions with broad implications in RNA splicing and translation.

Graphical abstract



Introduction

RNA metabolism is fundamental to cell differentiation and tissue development. Tight regulation of RNA metabolism is orchestrated by numerous RNA-binding proteins and dynamic RNA secondary structures (1–3). Ser/Arg-rich (SR) proteins are a family of RNA-binding proteins that regulate alternative splicing (4–8), a process that governs 95% of human genes, enabling 20000 protein-encoding genes to produce 200 000 protein isoforms (9–12). The SR protein family consists of 12 members (SRSF1–SRSF12), each featuring one to two N-terminal RNA recognition motifs (RRMs) and a phosphorylatable C-terminal protein region rich in repetitive Arg/Ser dipeptides (RS) (13,14). SR proteins typically

recognize exonic splicing enhancers and promote inclusion of bound exons, although recent studies have found that the effects of SR proteins depend on where they bind. For example, binding of SR proteins to introns inhibits the use of the neighboring splicing site for some RNA transcripts (15). In addition to their roles in regulating RNA splicing, SR proteins also affect genome stability (16), mRNA transcription (17,18), mRNA transport (19), translation (20,21), nonsense-mediated mRNA decay (22) and regulation of long noncoding RNA (23,24).

The RRM domains of SR proteins exhibit distinct but broad RNA-binding specificities, believed to play a dominant role in determining the RNA motifs that SR proteins

Received: October 18, 2023. Revised: February 28, 2024. Editorial Decision: March 6, 2024. Accepted: March 13, 2024

© The Author(s) 2024. Published by Oxford University Press on behalf of Nucleic Acids Research.

This is an Open Access article distributed under the terms of the Creative Commons Attribution License (<http://creativecommons.org/licenses/by/4.0/>), which permits unrestricted reuse, distribution, and reproduction in any medium, provided the original work is properly cited.

recognize. For instance, SRSF1 contains two RRM (RRM1 and RRM2, in a tandem configuration). RRM1 prefers C-containing RNA motifs (25), while RRM2 prefers GGA motifs (26,27) (Figure 1A). Consequently, SRSF1's RRM tandem recognizes purine-rich RNA motifs with upstream or downstream C motifs (25,28). Unlike SRSF1, SRSF3's RRM recognizes pyrimidine-rich RNA sequences (29). Due to their broad specificity, each SR protein can govern processing of many mRNA transcripts. For instance, SRSF1 alone affects the splicing of over 1500 RNA transcripts (30).

RS regions within SR proteins exhibit diverse lengths, ranging from 50 amino acids in SRSF1 to around 300 amino acids in SRSF4. Most RS dipeptide repeats in SR proteins undergo varying degrees of phosphorylation on serine residues. For example, the RS region of SRSF1 can exist in an unphosphorylated state, be partially phosphorylated (with the addition of 12 phosphate groups), or become hyperphosphorylated (with the addition of 18 phosphate groups). These RS regions are widely thought to interact with other protein factors that participate in splicing, such as U1 and U2 particles (31–41). Furthermore, these interactions are regulated by phosphorylation or dephosphorylation, which are pivotal in coordinating the spliceosome assembly and activation (31–41). Notably, RS regions of SR proteins potentially engage in RNA binding. A UV crosslinking experiment has shown a direct interaction of RS with RNA (42,43). Studies on IgM splicing have highlighted the indispensability of RS regions, as the exonic splicing enhancer presents sub-optimal binding sites for RRM (44–46). RS regions are also present in a larger family called SR-like proteins, which are extensively involved in RNA processing (39, 47–49). These observations hint at the potential role of RS regions as crucial RNA-binding components.

RNA metabolism is also subject to regulation by RNA structure, with one RNA structure garnering increasing attention: G-quadruplexes (GQs). In a GQ, four guanine bases form a planar array known as a G-tetrad via Hoogsteen base pairing. Typically, three or more layers of G-tetrads stack to create a GQ structure. Mono cations reside between G-tetrad layers, bonding with carbonyl oxygen atoms of guanines, and their stabilization of GQ follows an order of $K^+ > Na^+ > Li^+$. GQ structures can arise from both DNA and RNA sequences, and accumulating evidence underscores their roles in governing RNA transcription, stability, and RNA translation. Recent genome-wide exploration unveiled the presence of tens of thousands of GQs within the human transcriptome, with higher enrichment near exon-intron boundaries, implicating their involvement in alternative splicing (50). Despite the abundance of GQ-promoting sequence motifs, only a fraction of G-rich sequences yield functional GQ structures within cells (51). Remarkably, certain GQ formations are exceptionally stable, necessitating mechanisms to curtail extensive GQ assembly (52). Several RNA-binding proteins participate in this regulation. For example, hnRNPH1 has demonstrated its ability to inhibit GQ formation (53). Nevertheless, hnRNPH1's RNA recognition is limited to a small subset of RNA molecules. The identity of other proteins that share this regulatory role remains unknown. Recent investigations have uncovered that SR proteins, among numerous other proteins, can be recruited by a GQ-forming RNA from actin related protein complex subunit 2 (ARPC2), which regulates actin polymerization and cell migration (54). The ARPC2 GQ is in the 5' untranslated region of the ARPC2 mRNA. However, questions regarding the specificity of binding, the essen-

tial protein domains for GQ interaction, and the implications of this binding on ARPC2's GQ structure are still unanswered.

With our recent success in obtaining soluble full-length SRSF1, we use multiple biophysical methods to characterize the RNA-binding specificity of the RS region of SRSF1 and investigate the interaction between SRSF1 and the ARPC2 GQ. Contrary to the prevalent belief that the RS region has no RNA-binding specificity, we find that the SRSF1 RS prefers purine-rich RNA. We show that SRSF1 binds with ARPC2 GQ with a nanomolar affinity, and both the RRM tandem and RS are needed for GQ binding. Using fluorescence resonance energy transfer (FRET), we find that SRSF1 unfolds the ARPC2 GQ. This finding is further confirmed by circular dichroism. Interestingly, the RS region plays a dominant role in unfolding the ARPC2 GQ. Moreover, we show that SRSF1 can also bind and unfold other RNA GQs, such as MMP16 GQ and TERRA GQ. Through mutagenesis, we found that arginine residues in RS are responsible for the unfolding of GQ. We further use saturation transfer difference (STD) NMR to show that arginine sidechains interact with guanine bases but not with other nucleotide bases, providing an atomic-level mechanism for GQ unfolding by RS regions. Our luciferase assays suggest that the ARPC2 GQ inhibits the Renilla luciferase expression, which is consistent with the typical effect of GQs in 5' untranslated regions of mRNA on gene expression. Interestingly, this inhibition can be rescued by co-expression of full-length SRSF1 but not the RRM tandem, suggesting the crucial role of RS. In summary, our study reveals a new function of SR proteins in binding and unfolding GQ RNA, indicating a broad impact in regulating RNA metabolism given the prevalence of GQ and SR proteins.

Materials and methods

Synthetic RNA oligonucleotides

Synthetic 5' fluorescein-labeled RNAs: ARPC2, 5'-GGGGCUGGGCGGGACCGGG-3'; ARPC2 GQ mutant, 5'-GUAGACUGAGCGAAGACCGAG-3'; 21-mer GA, 5'-GAGAGAGAGAGAGAGAGAGAG-3'; MMP16, 5'-UUGGGAGGGAGGGAGAGGGUU-3'; TERRA, 5'-UGGGUUAGGGUUAGGGUUAGGG-3'; 21-mer CU, 5'-CUCUCUCUCUCUCUCUCUCUCUC-3'; 5'-UUCAGAGGA-3'; 5'-UCAGAGGG-3'; 8G, 5'-GGGGGGGG-3'; 8C, 5'-CCCCCCCC-3'; 8U, 5'-UUUUUUUU-3'; 8A, 5'-AAAAAAAA-3'; 4GA, 5'-GAGAGAGA-3'; 4CU, 5'-CUCUCUCU-3'.

Synthetic Cy3–Cy5 or Cy3 labeled RNA: Cy3–Cy5 ARPC2 GQ, 5'-Cy5-UGGGGGCUGGGCGGGACCGGGU-Cy3-3'; Cy3-ARPC2 GQ, 5'-UGGGGGCUGGGCGGGGACCGGGU-Cy3-3'; Cy3–Cy5 MMP16 GQ, 5'-UUAGUU-Cy5-UUGGGAGGGAGGGAGAGGGUU-Cy3-3'; Cy3–Cy5 TERRA GQ, 5'-UUAGUU-Cy5-UGGGUUAGGGUUAGGGU-Cy3-3'.

All RNA sequences, except for Cy3–Cy5 labeled RNA, were purchased from Dharmacon and dissolved in H₂O to achieve a concentration of 400 μM. G-quadruplex formation of all 21-mer RNA and ARPC2 RNA (200 μM) was carried out in the folding buffer containing 20 mM Tris–HCl, pH 7.5, 25 mM KCl and 0.1 mM EDTA. RNA was folded using a thermocycler by heating the RNA at 95°C for 5 min, followed by an annealing gradient to 4°C at a rate of 1°C/min. Folded RNA used in FP assays, CD, and UV melting experiments were

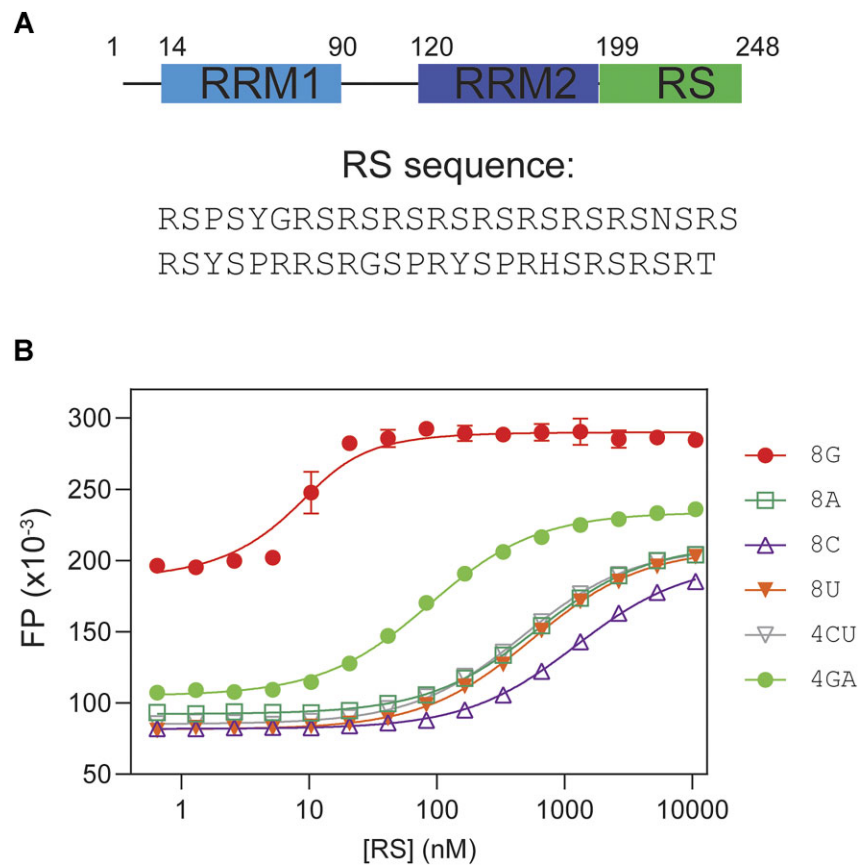


Figure 1. SRSF1 RS prefers purine ribonucleotides. **(A)** Domain architecture of SRSF1. The residue numbers are shown for these domain boundaries. The RS sequence (residues 198–248) is shown below. **(B)** Fluorescence polarization binding profiles for RS with various 8-mer RNA nucleotides. RNA oligomers were labeled by fluorescein at the 5' end, and fluorescent probe concentration was 10 nM for all binding assays. The binding assays were performed in a buffer containing 35 mM K_3PO_4 , 2.5 mM NaCl, 15 mM HEPES pH 7.5, 0.015% Tween 20, 0.075 mM TCEP.

diluted in 25 mM KCl, 0.25 M Arg/Glu, 20 mM Tris-HCl pH 7.5, 0.1 mM EDTA, 0.1 mM TCEP, 0.02% Tween 20, to achieve the concentration required for each experiment. Cy3-Cy5 or Cy3-labeled RNA (Integrated DNA Technology, IDT) was first dissolved in H_2O to achieve a concentration of 100 μM , and folded following the same procedure as stated above.

Molecular cloning and protein expression

The human SRSF1 gene (residues 1–248) was cloned into pSMT3 using BamH I and Hind III. The RRM tandem (residues 1–196), the RS region (residues 199–248), and their mutants were prepared using mutagenesis PCR. All SRSF1 constructs were expressed by BL21-CodonPlus (DE3) cells cultured in LB media at 37°C. Once the cell density reached an OD_{600} of 0.6, 0.5 mM of isopropyl thio- β -galactoside (IPTG) was added to induce protein expression at 22°C for 16 hours. The cells were then collected by centrifugation at 3000 RCF for 15 min.

Purification of the RRM-tandem constructs

Cell pellets were re-suspended in a lysis buffer containing 20 mM Tris-HCl, pH 7.5, 2 M NaCl, 25 mM imidazole, 0.2 mM TCEP, 1 mM PMSF, 0.5 mg/ml lysozyme, and 1 tablet of protease inhibitor. Cell lysate was sonicated after 3 freeze-thaw cycles and centrifuged at 23710 RCF for 40 min using a Beckman Coulter Avanti JXN26/JA20 centrifuge. The supernatant was loaded onto 5 ml of HisPur Ni-NTA resin

and washed with 200 ml of 20 mM Tris-HCl, pH 7.5, 2 M NaCl, 25 mM imidazole, and 0.2 mM TCEP. The sample was then eluted with 30 ml of 20 mM 2-morpholinoethanesulfonic acid sodium salt (MES), pH 6.5, 500 mM imidazole, 500 mM Arg/Glu and 0.2 mM TCEP. The eluted sample was cleaved with 2 $\mu g/ml$ Ulp1 for 2 h at 25°C (This step was skipped during the purification of SUMO tagged tandem RRMs and its RRM1 and RRM2 mutants) and diluted by threefold with a buffer A of 20 mM MES, pH 6.0, 100 mM Arg/Glu, and 0.1 mM TCEP before loading onto a 5-ml HiTrap Heparin column. The sample was eluted over a gradient with a buffer B of 20 mM MES, pH 6.0, 100 mM Arg/Glu, 0.1 mM TCEP, 2 M NaCl and 0.02% NaN_3 . Tandem RRM constructs were eluted around 50% B. Fractions containing the target proteins were pooled, concentrated, and loaded onto a HiLoad 16/600 Superdex 75 pg size exclusion column equilibrated with 20 mM Tris-HCl pH 6.5, 0.4 M Arg/Glu and 0.2 mM TCEP.

Purification of SRSF1

Cell pellets were re-suspended in a lysis buffer containing 20 mM Tris-HCl, pH 7.5, 150 mM Arg/Glu 2 M NaCl, 25 mM imidazole, 0.2 mM TCEP, 1 mM PMSF, 0.5 mg/ml lysozyme and 1 tablet of protease inhibitor. Cell lysis followed by Ni-purification and SUMO cleavage were carried out in the same manner as the purification of RRM-tandem constructs. Then the protein eluted from the Ni column was diluted by threefold with a buffer A of 20 mM MES, pH 4.6, 100 mM

Arg/Glu and 0.1 mM TCEP before loading onto a 5-ml HiTrap Heparin column. The sample was eluted over a gradient with a buffer B of 20 mM MES, pH 11.5, 400 mM Arg/ Glu, 0.1 mM TCEP, 2 M NaCl and 0.02% NaN₃ in which the protein was eluted around 85% B. Fractions containing the target proteins were pooled, and pH was adjusted to 6.0–8.0 followed by concentration. The sample was exchanged to a buffer containing 20 mM Tris–HCl pH 7.5, 0.80 M Arg/Glu, 0.2 mM TCEP and concentrated.

Purification of RS tail constructs

Cell pellets were re-suspended in a lysis buffer containing 20 mM Tris–HCl, pH 7.5, 25 mM imidazole, 0.1 mM TCEP and 6 M Guanidinium HCl. Cell lysate was sonicated after 3 freeze-thaw cycles and centrifuged at 23710 RCF for 40 min using a Beckman Coulter Avanti JXN26/JA20 centrifuge. The supernatant was loaded onto 5 ml of HisPur Ni-NTA resin and washed with 200 ml of 20 mM Tris–HCl, pH 7.5, 0.2 mM TCEP and 25 mM imidazole. The sample was then eluted with 30 ml of 500 mM Arg/Glu, pH 7.0, 500 mM Imidazole, 1 mM TCEP, and 1 protease inhibitor cocktail. The eluted sample was cleaved with 2 µg/ml Ulp1 for 1 h at 37°C and diluted by twofold with a buffer A of 20mM sodium acetate, pH 5.0, 0.2 mM TCEP before loading onto a 5-ml HiTrap SP column. The protein was eluted over a gradient with a buffer B of 20 mM sodium acetate, pH 5.0, 2 M NaCl, and 0.2 mM TCEP. RS tail constructs were eluted approximately 30% B. Fractions containing the target proteins were pooled and concentrated. The concentrated proteins were exchanged and concentrated into a buffer containing 20 mM Tris–HCl, pH 7.5 and 0.2 mM TCEP.

CD spectroscopy

CD spectroscopy was employed to test the conformation of folded RNA using a JASCO J-815 CD spectrometer. CD spectra of all folded 21-mer RNA (5 µM) were collected at 25°C in 25 mM KCl, 0.25 M Arg/Glu, 20 mM Tris–HCl, pH 7.5, 0.1 mM EDTA, 0.1 mM TCEP, and 0.02% Tween 20. Another set of CD spectra of the folded ARPC2 GQ RNA was collected at 25°C and 95°C in a 25 mM KCl without Tween 20. The CD spectrum of the 10 µM 8G RNA (unfolded) was collected in a 35 mM potassium phosphate buffer (35 mM K₃PO₄, 2.5 mM NaCl, 15 mM HEPES pH 7.5, 0.015% Tween 20 and 0.075 mM TCEP).

CD spectra were collected for the ARPC2 GQ RNA sample at a concentration of 5 µM, in the presence of varying concentrations of the RRM tandem (ranging from 2.5 to 15 µM). All the CD spectra were scanned three times to obtain spectral average using a 10-mm path length cuvette and a scanning speed of 50 nm/min, covering a wavelength range of 200–320 nm. Corresponding buffer spectra were subtracted for baseline correction.

UV melting

UV melting and annealing experiments were conducted using 10-mm path length quartz cells on a JASCO V-730 spectrophotometer with a sample volume of 1.5 ml. The quartz cells were sealed to prevent the sample evaporation. Folded RNA was diluted to 5 µM in a buffer containing 25 mM KCl, 0.25 M Arg/Glu, 20 mM Tris–HCl, pH 7.5, 0.1 mM EDTA and 0.1 mM TCEP. The absorbance at 295 nm was recorded after heating to 95°C, followed by cooling to 25°C

at a 0.2°C/min temperature gradient. The annealing and melting cycles were carried out in triplicate as three independent experiments.

FP assays

Fluorescence assays for 8-mer RNA were collected in 35 mM K₃PO₄, 2.5 mM NaCl, 15 mM HEPES pH 7.5, 0.015% Tween 20, and 0.075 mM TCEP. Fluorescence polarization assays for 21-mer RNA were performed in 25 mM KCl, 0.25 M Arg/Glu, 20 mM Tris–HCl pH 7.5, 0.1 mM EDTA, 0.1 mM TCEP, and 0.02% Tween 20. Ten nM of 5' fluorescein-labeled RNA was mixed with proteins at concentrations ranging from 8000 nM to 0.488 nM, in black flat-bottom 96-well plates (Costar). Protein-RNA mixtures (50 µl) were shake at 100 RPM for 10 min, followed by incubation at 37°C for 30 min, and then at 25°C for 10 min. Fluorescence polarization measurements were carried out using a Cytation 5 with an excitation wavelength of 485 nm and an emission wavelength of 520 nm. We have shown that the total fluorescence intensities did not change during protein titration. Therefore, the dissociation constants (K_D) were fitted using the quadratic equation with assumption of one-site interaction. The fluorescence polarization (F_p) binding curves were fitted using the quadratic equation below, where the fitting parameters F_{min} , F_{max} and K_D represent the fluorescence polarization baseline, plateau, and dissociation constant, respectively. $[P_T]$ represents the total protein concentration and $[L_T]$ represents the total RNA concentration (10 nM). Errors in dissociation constants were calculated based on three independent measurements.

$$F_p = F_{min} + (F_{max} - F_{min}) \times \frac{([P_T] + [L_T] + K_D) - \left(([P_T] + [L_T] + K_D)^2 - 4[P_T][L_T] \right)^{0.5}}{2[L_T]} \quad (1)$$

Fluorescence spectroscopy

The Cy3–Cy5 labeled RNA (200 nM) was dissolved in 100 µl of 25 mM KCl, 0.25 M Arg/Glu, 20 mM Tris–HCl, pH 7.5, 0.1 mM EDTA, and 0.1 mM TCEP. RS, the RRM tandem, KS or RA stock solution (20 µM) dissolved in 20 mM Tris–HCl, pH 7.5, 0.4 M Arg/Glu, 0.1 mM TCEP was titrated into GQ RNA. Fluorescence emission spectra of protein-bound RNA were recorded from 530 to 700 nm using a Cytation 5 in black flat-bottom 96-well plates (Costar) at 25°C. Full-length SRSF1 phase separates upon titrated into GQ RNA. To eliminate interference of phase separation, the SRSF1 RNA mixtures were centrifuged at 16 000 RCF for 10 min, and supernatants were used for fluorescence spectrum collection. Fluorescence emission spectra of the apo RNA were collected immediately after denaturation at 95 °C for 5 min. Samples were excited at 500 nm, and we have confirmed that this wavelength did not excite Cy5. All fluorescence spectra were collected in triplicate, and the average emission intensities were normalized by the Cy3 signal maximum at 566 nm after subtraction of baseline.

Saturation transfer difference NMR

Mixtures of 500 µM 3-mer RNA oligomers and 10 µM RS were prepared in a D₂O buffer with a pH of 5.6, supplemented with 1 mM MES. To eliminate residual H₂O, the samples were freeze-dried and subsequently re-dissolved in 99.9% D₂O. STD-NMR data were acquired at 298 K using an 850 MHz

magnet and the sequence previously reported (55). A total of 16 transients were accumulated for all experiments.

Plasmid design for dual luciferase assay, western blot and RT-PCR

The ARPC2 GQ DNA or 21-mer CU repeats sequence was introduced upstream of the Renilla luciferase gene of the psiCHECK2 plasmid via two separate mutagenesis polymerase chain reactions, with the first and second halves of the ARPC2 GQ introduced to the NheI restriction site downstream of the T7 promoter. The DNA encoding human SRSF1 was cloned into the pcDNA4 myc His A plasmid using BamH I and Hind III. Using mutagenesis polymerase chain reaction, pcDNA4 containing DNA encoding the RRM tandem was constructed.

Cell culture and transfection

HEK 293 cells were cultured in Dulbecco's Modified Eagles medium (DMEM) containing 10% fetal bovine serum (FBS) and 1% penicillin and streptomycin. Cells were grown at 37°C in an incubator containing 5% CO₂ and passaged into new media in a 6-well plate every 2–3 days. Cells were inoculated in 96 well-plates prior to the transfection for the dual Luciferase assay. Once the cells reached 60–70% confluency, cells were transfected with wild-type psiCHECK2, psiCHECK2-ARPC2 GQ, psiCHECK2-ARPC2 CU, pcDNA4-SRSF1 or pcDNA4-RRM tandem using LipofectAMINE 3000 (Invitrogen) according to the manufacturer's instructions. After transient transfection, cells were incubated at 37°C for 48 h until the cell density reached a confluency of about 95%.

Dual luciferase assay

Dual luciferase assays were conducted after lysing the transfected cells using the Dual-luciferase Reporter Assay kit (Promega) according to the manufacturer's instructions. The firefly and Renilla luciferase activities of each tested condition were measured in three independent replicates using a Cytation 5 plate reader. The average luciferase activity was determined as the ratio of Renilla to firefly luciferase activity. The Renilla/firefly luminescence ratio of psiCHECK2-GQ and psiCHECK2-CU were used to normalize other datasets.

Western blot

Western blots were carried out after the lysis of the transfected cells with SDS-PAGE loading buffer. Western blots were conducted as previously described (56). SRSF1 and the RRM tandem were immunoblotted with a primary antibody called Goat anti-ECS (DYKDDDDK) and Anti Goat, a secondary antibody conjugated with horseradish peroxidase (HRP). Antigen-antibody complexes were visualized by the SYNGENE gel imager and GeneSys gel imaging software.

Results

The RS region of SRSF1 demonstrates RNA binding specificity

Given that SRSF1 RS contains 19 arginine residues, it is intuitive to conceive that the RS region can contact nucleotides via electrostatic interactions. However, the RNA-binding specificity of RS has never been directly examined. To this end, we used fluorescence polarization (FP) to measure the binding

Table 1. RS prefers purine-rich RNA

Nucleotide	K_D (nM)
8G*	3.0 ± 0.8
8A	610 ± 15
8C	1220 ± 40
8U	550 ± 21
4CU	470 ± 12
4GA	83 ± 3

*8G RNA forms an intermolecular G-quadruplex, making FP values higher than other RNA oligomers in the single-stranded conformation.

affinities of RS to various RNA oligonucleotides (Figure 1A). To prevent protein RNA co-aggregation, which may interfere with binding assays, we carefully chose the RNA lengths and salt concentrations.

We found that 8-mer RNA did not aggregate in a buffer containing 35 mM potassium phosphate (Supplementary Figure S1A). In searching for the optimal salt concentration for binding assays, we found that salts significantly weakened the interaction between RS and RNA, suggesting a role of electrostatic interactions in RS and RNA binding (Supplementary Figure S1B). Of all tested RNA, RS had the highest affinity to 8-mer poly-G. We found that 8-mer poly-G formed intermolecular G-quadruplex, as shown by the diagnostic negative peak at 240 nm and the positive peak at 267 nm (Supplementary Figure S1C). Therefore, its binding affinity to RS cannot be compared with other 8-mer single-stranded RNA due to differences in structure and net charges. As a substitute for 8-mer poly-G, we tested 8-mer GA, which is unable form GQ. Apart from 8-mer poly-G, RS bound more tightly to 8-mer GA than to 8-mer CU or other polymers (Figure 1B, Table 1). Therefore, we concluded that RS preferred purine rich sequences. As the nucleotides tested here had the same number of backbone phosphates, the difference in RS binding affinity was attributed to nucleobases.

Both the RS and the tandem RRM are essential for RNA GQ binding of SRSF1

The 5' untranslated region of human ARPC2 mRNA contains a 21-nucleotide sequence that forms G-quadruplex (ARPC2 GQ) (Figure 2A). A previous study has found that ARPC2 GQ can pull down SRSF1, along with other SR proteins (54). Our success in obtaining soluble SRSF1 gave us an opportunity to quantitatively examine this interaction and to investigate which SRSF1 domains are responsible for the GQ binding. To this end, we carried out FP assays in a buffer that contained 25 mM KCl and 250 mM Arg/Glu. Arg/Glu was used to prevent phase separation, which may interfere with FP assays or circular dichroism (CD) characterization. We confirmed that the ARPC2 GQ RNA was successfully folded into G-quadruplex in the presence of 25 mM KCl, as suggested by the negative peak around 240 nm and the positive peak around 267 nm in the CD spectrum (Figure 2B). The presence of Arg/Glu did not change the CD spectrum of the ARPC2 GQ (Supplementary Figure S2A). The formation of GQ was further confirmed by the characteristic UV melting curve monitored at 295 nm (Supplementary Figure S2B).

In this buffer, SRSF1 bound with ARPC2 GQ with a K_D of 4 nM (Figure 2C, Table 2). RS or the RRM tandem alone bound to the GQ RNA with a much lower affinity (K_D is around 200 nM). However, the RRM1/RRM2 linker has no

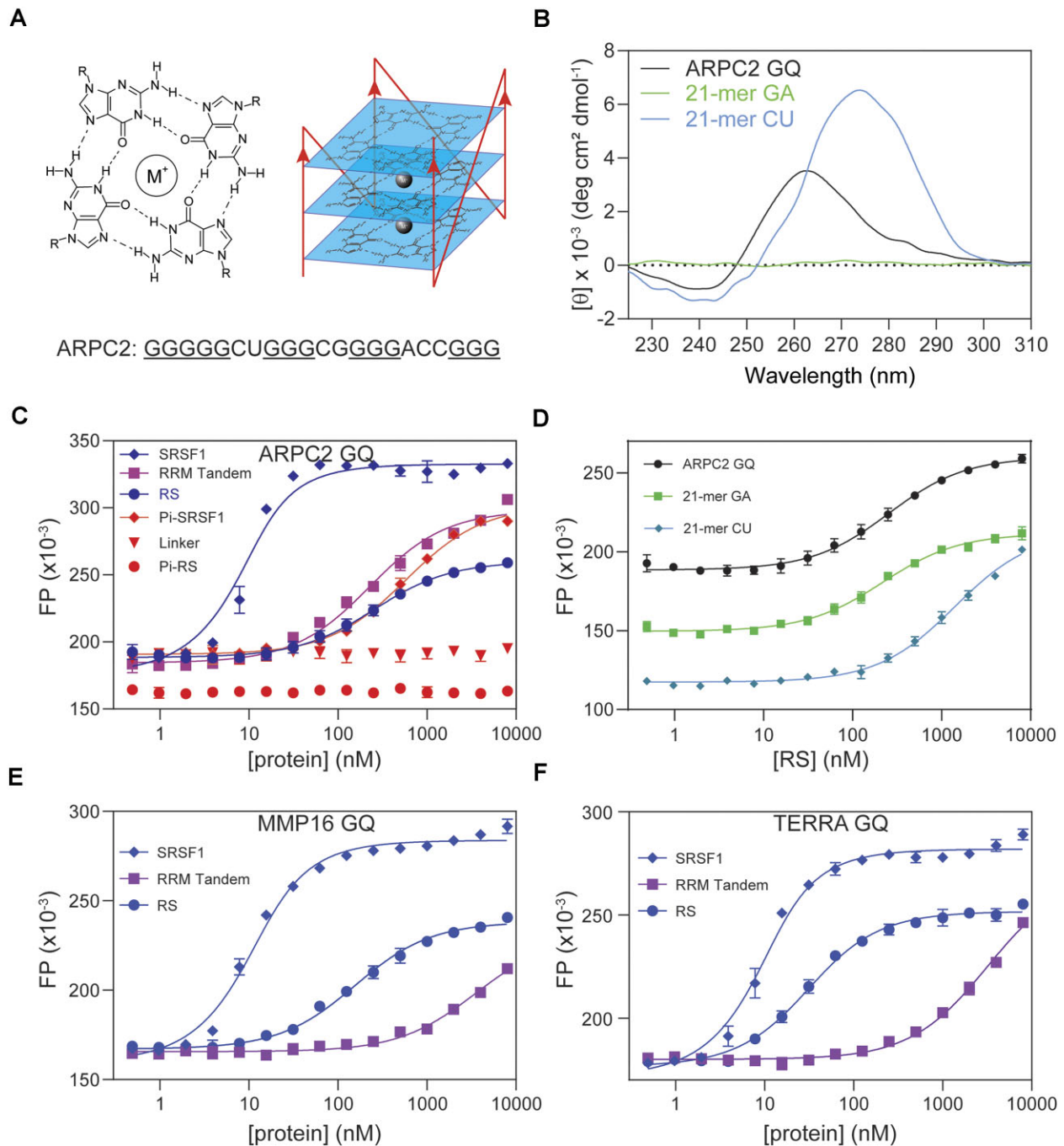


Figure 2. Both RS and the RRM tandem of SRSF1 contribute to its interaction with the ARPC2 GQ. **(A)** Schematic diagram of G-quadruplex. M⁺ denotes mono cations. A parallel GQ is shown on the right. Mono cations lay between G-tetrad layers and form bonds with carbonyl oxygen atoms. The ARPC2 GQ sequence used in this study is shown below. Putative guanine residues that are involved in forming G-tetrads are underlined. **(B)** The circular dichroism spectrum of the ARPC2 GQ. **(C)** FP binding curves of the ARPC2 GQ with various SRSF1 constructs. **(D)** FP binding curves for RS with 21-mer GA, 21-mer CU, and the ARPC2 GQ. FP binding curves of SRSF1, the RRM tandem, and RS with MMP16 GQ **(E)** and TERRA GQ **(F)**. FP measurements were performed in a buffer containing 25 mM KCl, 0.25 M Arg/Glu, 20 mM Tris-HCl pH 7.5, 0.1 mM EDTA, 0.1 mM TCEP, 0.02% Tween 20. Fluorescein was attached to the 5' end of RNA, and the probe concentration was 10 nM for all samples.

detectable binding to the ARPC2 GQ (Figure 2C). These results together suggested that both the RRM tandem and RS were necessary for the ARPC2 GQ binding. As RS is subject to phosphorylation in the cell, we further tested how phosphorylation affected its GQ binding and found that hyperphosphorylation of RS completely abolished its binding to GQ (Figure 2C). Different from isolated RS, hyper-phosphorylated SRSF1 binds to ARPC2 GQ with a lower affinity than the RRM tan-

dem (K_D of 570 nM versus 220 nM), suggesting that phosphorylation not only abolishes RS RNA binding, but also inhibits RNA binding of the neighboring RRM tandem (Figure 2C).

Using 8-mer RNA, we showed that RS preferred purine-rich RNA. We wondered whether this RNA-binding preference remained for longer RNA. To this end, we compared binding affinities to ARPC2 GQ (21-mer), poly-GA or CU of the same length. Consistent with our findings using 8-mer RNA, the

Table 2. Both the RRM tandem and the RS region of SRSF1 contribute to its interaction with the ARPC2 GQ

Protein constructs	RNA	K_D (nM)
SRSF1	ARPC2 GQ	3.6 ± 0.7
RS	ARPC2 GQ	250 ± 22
RRM Tandem	ARPC2 GQ	220 ± 19
RRM1/RRM2 linker	ARPC2 GQ	No binding
Pi-SRSF1	ARPC2 GQ	570 ± 35
Pi-RS	ARPC2 GQ	No binding
RS	21-mer GA	210 ± 16
RS	21-mer CU	1400 ± 100
SRSF1	MMP16 GQ	5.9 ± 0.6
RS	MMP16 GQ	150 ± 10
RRM Tandem	MMP16 GQ	3500 ± 490
SRSF1	TERRA GQ	4.6 ± 0.5
RS	TERRA GQ	26 ± 2
RRM Tandem	TERRA GQ	3200 ± 290

binding affinity of RS to 21-mer GA is 7-fold higher than that to 21-mer CU (K_D of 210 ± 16 nM versus 1400 ± 100 nM). RS binds to the ARPC2 GQ with a similar K_D to 21-mer GA. Notably, 21-mer GA did not form GQ, according to our CD data (Figure 2D). These results suggest that RS prefers guanine rich RNA sequences regardless of their secondary structure.

To assess the binding capability of SRSF1 with other RNA GQs, we chose two orthologous RNA sequences: MMP16 GQ and telomeric repeat-containing RNA (TERRA GQ). These two RNA sequences do not possess cytidine for RRM1 recognition. Previous research has demonstrated SRSF1's interaction with MMP16 GQ (54), while TERRA is known for its GQ formation and involvement in telomere maintenance (57). We found that SRSF1 binds to both RNA GQs with comparable affinity to ARPC2 GQ (Table 2 and Figure 2E, F). RS exhibited a binding affinity to MMP16 GQ akin to ARPC2 GQ, whereas it has a higher affinity to TERRA GQ. Interestingly, the binding affinities of the RRM tandem to MMP16 and TERRA GQs were approximately 15-fold weaker compared with ARPC2 GQ (Figure 2E, F).

Identification of key SRSF1 residues responsible for ARPC2 GQ binding

We have shown that both the RRM tandem and RS are required for ARPC2 GQ binding. To understand the binding mechanism, we wanted to identify the SRSF1 residues essential for ARPC2 GQ binding. RRM1 and RRM2 of SRSF1 recognize C- and GGA-containing single-stranded RNA motifs, respectively (25,26). These motifs are also present in ARPC2 GQ. Others and our studies have identified the SRSF1 residues for RNA binding, such as Y19, F56, F58, W134 and Q135 (Figure 3A and B) (26,28). In our previous study, we have confirmed that mutation of these residues does not perturb the protein structure (28). Therefore, we compared binding affinities of the wild-type RRM tandem with its mutants. R173 of RRM2 is distal to its RNA-binding site and was selected as a negative control. We found that the SRSF1 residues essential for binding to classic RNA ligands were also important for ARPC2 GQ binding (Table 3, Figure 3B and C), suggesting that the RRM tandem recognizes ARPC2 GQ via the binding sites for single-stranded RNA (ss-RNA). These residues form either stacking interactions (Y19, F56, F58, W134) or H-bonds (Q135) with nucleobases of ss-RNA. The results of RRM1 mutants are also in line with those binding data for

MMP16 and TERRA GQs (Table 2, Figure 2E and F). Unlike ARPC2 GQ, MMP16 and TERRA GQs have no cytidine base that is specifically recognized by RRM1, which explains their lower binding affinities to the RRM tandem.

GQ-forming sequences usually contain at least four G-tracts of three consecutive guanines. Therefore, it is of interest to test whether the SRSF1 tandem RRMs binds with the GGG motifs, in addition to its optimal motif GGA. Therefore, we used the GGG motif to replace the GGA motif of UCA-GAGGA, one of classic consensus RNA ligands for SRSF1. We found that replacement of GGA by GGG only reduced binding affinity by three-fold. Therefore, it is possible that RRM2 either binds to GGA or GGG if these sites are exposed. In summary, our results suggest that the SRSF1 RRM tandem uses its classic RNA-binding sites to bind with C- and GGA-/GGG-containing motifs.

In the previous sections, we showed that RS demonstrated RNA-binding specificity, and this specificity is unlikely attributed to charge-charge interaction. SRSF1 RS contains 19 arginine residues and 20 serine residues, accounting for three quarters of its amino acid composition. We wondered what residues are responsible for the RS and ARPC2 GQ binding. To this end, we created two RS mutants, KS and RA, in which all arginine or serine residues were replaced by lysine (the KS mutant) or alanine (the RA mutant), respectively (Figure 4A). The KS mutant has the same charge distribution as RS. However, its binding to ARPC2 GQ was too weak to be detected (Figure 4B). In contrast, RA showed a similar RNA-binding affinity to RS (Figure 4B). These results suggest that arginine residues in RS are the main contributors to its GQ binding.

SRSF1 unfolds ARPC2 GQ

RNA GQ is folded in such a way that the majority of guanine nucleobases are packed inside, while the phosphate backbones are exposed (Figure 2A). However, the RNA-binding specificity of the RRM tandem and RS requires nucleobases to be exposed. This implies that SRSF1 binding potentially unfolds the GQ. To test this hypothesis, we attached the 5' and 3' ends of ARPC2 GQ RNA with Cy5 and Cy3 fluorescent probes, respectively (Figure 5A). The formation of GQ allows fluorescence resonance energy transfer (FRET) between Cy3 and Cy5, which have a Förster range of 53 Å (58). We observed the Cy5 fluorescence emission at 670 nm when the sample was excited with light at 500 nm. We also confirmed that Cy5 alone was not excited by light at 500 nm (Figure 5A). Therefore, the observed FRET is attributed to GQ formation. To confirm that the Cy5 signal can be used to probe unfolding of GQ, we also collected a spectrum for the thermally denatured GQ, which has a lower Cy5 signal (Figure 5A). To rule out the possibility that Cy5 or Cy3 labeling affects GQ formation, we collected CD spectra and confirmed that fluorophore labeling did not disturb the GQ structure (Supplementary Figure S3A).

To avoid interference from potential phase separation or aggregation, we dissolved ARPC2 GQ and SRSF1 in a high ionic strength buffer containing 25 mM KCl and 0.25 M Arg/Glu and centrifuged the samples before collecting fluorescence data. This experiment design depends on the relative fluorescence intensity decrease of Cy5 to detect GQ unfolding. To rule out the possibility of fluorescence quenching by RS, we performed two control experiments. In the first control experiment, we compared the fluorescence spectra of Cy3- and Cy3/Cy5-labeled ARPC2 GQ. The Cy3

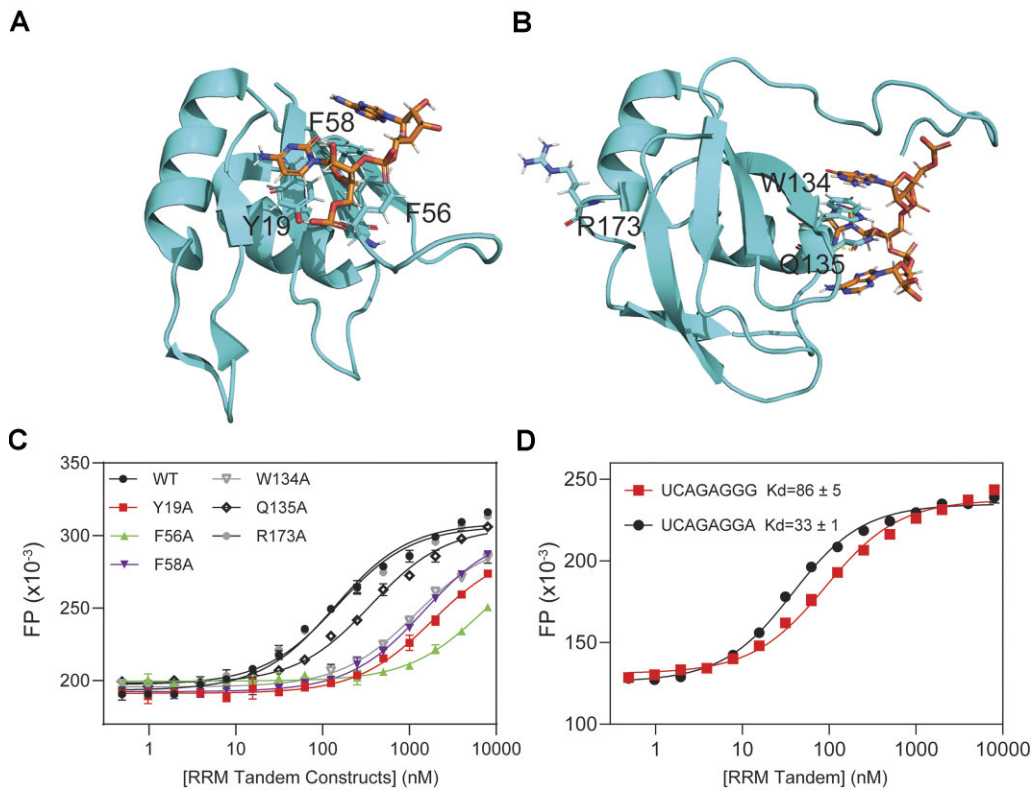


Figure 3. RRM1 and RRM2 residues for recognizing single-stranded RNA are also essential for ARPC2 GQ binding. **(A)** Structure of RRM1 (PDB ID: 6HPJ) and **(B)** RRM2 (PDB ID: 2M8D) with their cognate RNA motifs. RNA and protein residues are shown by orange and cyan sticks, respectively. Molecular graphics were prepared using PyMOL. **(C)** FP binding curves of ARPC2 GQ with the RRM tandem and its mutants. **(D)** FP binding curves of the RRM tandem with GGA and GGG motifs.

Table 3. The RRM tandem uses its classic RNA-binding sites for its interaction with the ARPC2 GQ

RRM tandem mutants	K_D (nM)	Relative K_D
WT	130 ± 11	1
RRM1 Y19A	1800 ± 160	14
RRM1 F56A	7000 ± 1500	54
RRM1 F58A	1500 ± 80	12
RRM2 W134A	1200 ± 90	9
RRM2 Q135A	350 ± 20	3
RRM2 R173A	140 ± 12	1

intensity of the single-labeled ARPC2 GQ is higher than that of double-labeled RNA (Figure 5B, blank versus green lines), as the Cy3 energy is transferred to Cy5 via FRET in the double-labeled RNA. Upon addition of RS (Figure 5B, purple line), the Cy5 signal decreases and the Cy3 signal increases relative to double-labeled the RNA GQ. These results suggest there is no signal quenching for Cy3. We further compared fluorescence intensity of Cy5 with and without RS and found that addition of RS enhanced instead of quenching the Cy5 signal (Supplementary Figure S3B).

An obvious decrease in the Cy5 signal was observed with gradual titration of SRSF1 (Figure 5C). It is noteworthy that the Cy5/Cy3 ratio for SRSF1-bound ARPC2 GQ was lower than that of the sample denatured at 95°C (Figure 5A), suggesting that SRSF1 is more efficient in unfolding ARPC2 GQ than thermal denaturation. We further investigated the roles of the RRM tandem and RS in unfolding GQ. We found that the RRM tandem decreased the Cy5 relative

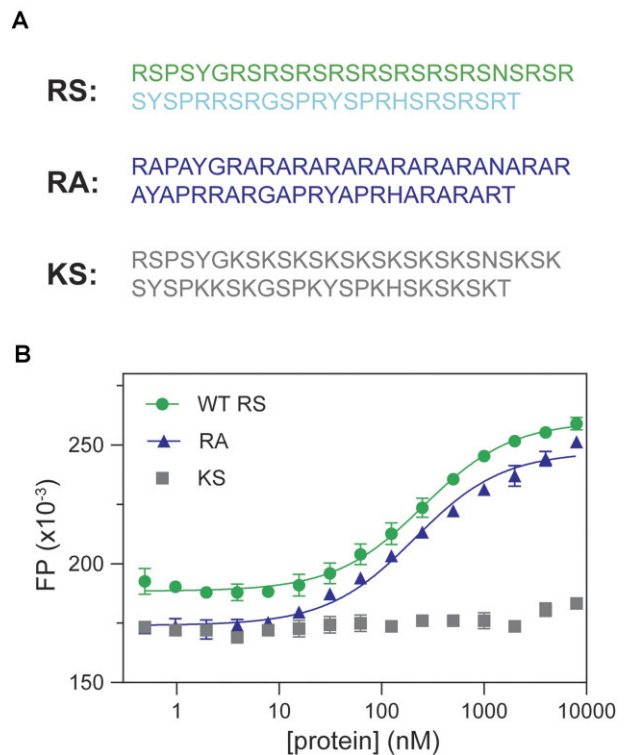


Figure 4. Arginine residues in RS are the main contributors for ARPC2 GQ binding. **(A)** Sequences of RS and its mutants, RA, and KS. ARPC2 GQ (10 nM) is labeled by fluorescein at the 5' end. **(B)** FP binding curves for ARPC2 GQ and RS, KS and RA.

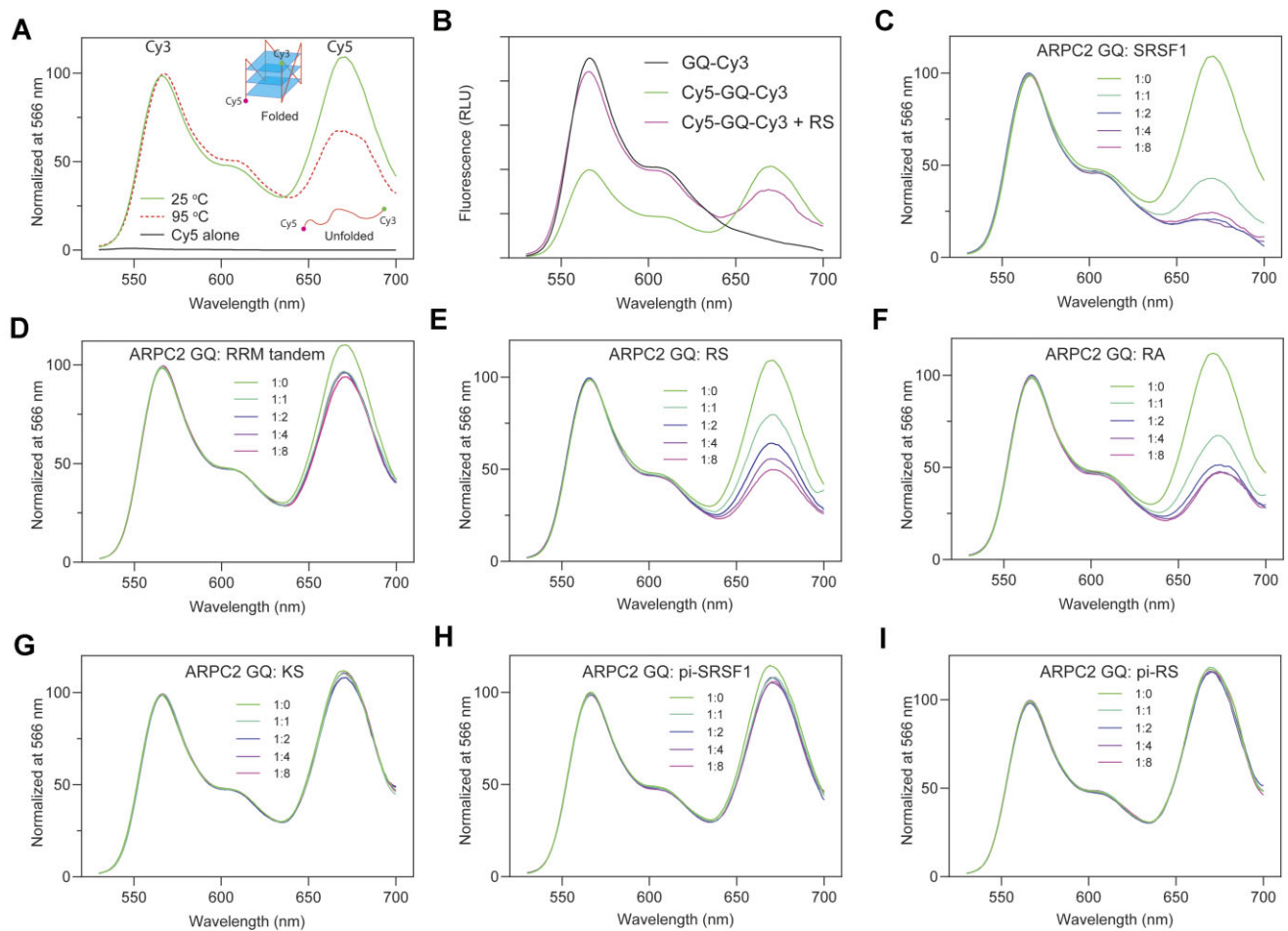


Figure 5. The RS region of SRSF1 plays a dominant role in unfolding ARPC2 GQ. **(A)** The principle of the experimental design. Cy5 and Cy3 were labeled at the 5' and 3' ends of ARPC2 GQ, respectively. When excited by light at 500 nm, the fluorescence spectrum of ARPC2 GQ demonstrated the Cy3 signal maxima at 566 nm and the Cy5 signal maxima at 670 nm due to FRET (green line). Thermally denatured GQ has a relatively lower Cy5 signal. Cy5 alone could not be excited by light at 500 nm (black line). **(B)** Control experiments to test whether RS quenches Cy3. The fluorescence spectra in the relative light unit (RLU) were normalized to the same RNA concentrations. Fluorescence spectra were collected when ARPC2 GQ was titrated with **(C)** full-length SRSF1, **(D)** the RRM tandem, **(E)** RS, **(F)** RA, **(G)** KS, **(H)** phosphorylated SRSF1 (pi-SRSF1) and **(I)** phosphorylated RS (pi-RS). All spectra were collected with excitation light at 500 nm and the ARPC2 GQ concentration is 200 nM.

signal by <20% (Figure 5D). This is consistent with our circular dichroism results, which showed a mild decrease in the GQ-characteristic peak around 267 nm (Supplementary Figure S3C). In contrast, RS unfolds ARPC2 GQ more efficiently (Figure 5E). In line with our binding assays (Figure 4B), the RA mutant can unfold ARPC2 GQ (Figure 5F), whereas KS cannot. (Figure 5G). As a negative control, we also tested BSA and found that it was unable to unfold ARPC2 GQ (Supplementary Figure S3D). Furthermore, phosphorylated SRSF1 (Figure 5H) or RS (Figure 5I) has lower efficiency in unfolding ARPC2 GQ, which agrees with our FP binding assays (Figure 2C).

We performed additional experiments to investigate the ability of SRSF1 to unfold MMP16 and TERRA GQs, which exhibit a strong binding affinity to SRSF1 (Figure 2E and F). The unfolding profiles of these two GQs closely resembled those observed for ARPC2 upon titration of SRSF1 and its domains (Supplementary Figure S3E and S3F). Both full-length SRSF1 and RS efficiently destabilized MMP16 and TERRA GQs, whereas the RRM tandem had a minimal impact on these RNA GQs (Supplementary Figure S3E, F). Taken together, these findings indicate the capacity of RS to unfold various RNA GQ structures.

The Arg sidechain interacts with the guanine base, which may be responsible for GQ unfolding

In previous sections, we have shown that RS has RNA-binding specificity, and Arg residues in RS play a main role in unfolding ARPC2 GQ. In addition to forming electrostatic interactions with phosphate backbones, arginine residues are also able to form H-bonding and stacking interactions with nucleobases. As RS unfolds GQ, the complex may exist in numerous conformations, which makes crystallography unsuitable. NMR is a powerful method to characterize dynamic interactions. However, RS and ARPC2 GQ phase separate at the concentration for NMR studies (> 50 μ M), making our system a difficult case. To avoid phase separation, we tested RNA homopolymers of different lengths and found that 3-mer polynucleotides remained soluble after being mixed with RS. This success enabled us to use saturation transfer difference (STD) NMR to characterize the interaction between RS and homo-polymeric RNA. STD NMR selectively saturates resonances of a functional group of one binder (usually large molecules). The saturation can be diffused to neighboring protons through intramolecular proton-proton cross relaxation. Due to transient interactions, the saturation can be transferred to the ligand via inter-molecular NOE, which

enables the identification of epitopes involved in binding (Figure 7A). STD is a sensitive method to detect weak binding with a K_D up to the millimolar range. If Arg sidechains interact with nucleobases, STD signal should be observed when saturation is applied to Arg sidechains. We irradiated methylene groups of Arg sidechains, whose NMR chemical shifts are clustered around 2.5 ppm, away from the chemical shift of nucleobases (>7.0 ppm). We collected STD data for 3-mer poly-A, C, G and U with sub-stoichiometric amount of RS. As shown by Figure 6B, GGG of the four 3-mer RNAs showed the strongest STD signals. CCC demonstrates much weaker STD signals, while poly-A and poly-U do not exhibit STD signals significantly higher than baseline noises. These results suggested that the guanine base was involved in interacting with the Arg sidechain. Our results also agree with a previous bioinformatic study that shows that the interaction between the Arg sidechain and guanine ranks the most probable one among protein DNA recognition (59).

SRSF1 alleviates translation inhibition induced by the ARPC2 GQ

The presence of GQs in mRNA typically impedes gene expression by creating steric hindrance. Previous studies have used dual luciferase assays to detect a 40% reduction in translation efficiency in the presence of ARPC2 RNA GQ (54). We hypothesized that if SRSF1 can unwind RNA GQs within the cell, it should be capable of rescuing the reduction in gene expression caused by GQ formation. To investigate this hypothesis, we introduced the ARPC2 GQ sequence upstream of the Renilla luciferase gene in the psi-CHECK2 plasmid (Figure 7A). As a negative control, we introduced a 21-mer long non-GQ forming sequence containing CU repeats to the exact same location in the psi-CHECK2 plasmid. The firefly luciferase gene within this plasmid served as a reference gene to standardize transfection efficiency. Additionally, we cloned SRSF1 or the RRM tandem into the pcDNA4 plasmid for co-transfection (Figure 7A).

Upon transfection of HEK293 cells with the psi-CHECK2 plasmid containing the ARPC2 GQ sequence, the ratio of luciferase activity between Renilla and firefly was reduced to 70% compared to empty psi-CHECK2 (psi, gray bar in Figure 7B), or the plasmid containing CU repeats of the same length as ARPC2 GQ (pc, Figure 7B). This is consistent with the previous study (54). Co-transfection of the cell with pcDNA4 encoding SRSF1 increases the luciferase activity, whereas the RRM tandem has no such effect. Notably, this rescuing effect of SRSF1 displayed dose-responsive behavior (Supplementary Figure S4A). Although SRSF1 boost gene expression for both psi-CU and psi-GQ, its effect on psi-GQ is significantly larger than that to psi-CU (Figure 7C, left two bars). As a control, RRM has the same effect on psi-CU and psi-GQ (Figure 7C, right two bars). We confirmed that the full-length SRSF1 and the RRM tandem were expressed using western blots (Supplementary Figure S4B). It's worth mentioning that the RS region is inherently unstructured and susceptible to degradation and modification within the cell, which is why we did not evaluate the co-transfection of the RS-encoding plasmid in the luciferase assays.

Discussion

RS regions are abundant in the human proteome, as exemplified by SR proteins and SR-like proteins. In SR proteins,

the primary function of RS regions has been found to mediate protein-protein interactions. Due to their extensive electropositive charges, RS regions are generally considered to have nonspecific and, in some cases, undesirable roles as RNA binders, often regarded as secondary in most scenarios. Indeed, the RS region of SRSF1 is unnecessary for splicing of RNA transcripts with robust splicing enhancers (26,60). Nevertheless, several studies have indicated that RS regions can play a role in RNA binding. Shen et al. have shown the crosslinking between RS regions and RNA transcripts (42,43). Moreover, RS regions are indispensable for RNA transcripts with weak splicing enhancers, such as IgM (42,46). Collectively, these studies suggest that RS enhances RNA binding of SRSF1. Our research has provided a new insight, revealing that RS regions exhibit binding preference for purine-rich RNA. Therefore, it is conceivable that RS regions not only enhance RNA binding but also fine tune the RNA-binding specificity of SRSF1.

The preference of RS for purine-rich RNA underpins its role in RNA GQ binding. A previous study has found that the ARPC2 GQ-forming region can pull-down most of SR family members (61). For SRSF1, the RRM tandem and the RS region have an overlapping binding specificity, which is coincidental. RRM domains from other SR proteins have distinct RNA-binding specificity. For example, the SRSF3 RRM prefers pyrimidine-rich RNA (29,62–64). Therefore, it is unlikely that all SR proteins depend on their RRM domains to binding RNA GQ. On the contrary, RS regions of SR proteins are shared across the family, suggesting RS regions are probably responsible for GQ binding for some SR proteins. This is in line with the aforementioned findings of RS/RNA crosslinking and RS-dependent splicing for some RNA transcripts (42,43,46). In addition, we showed that phosphorylation completely abolishes RNA binding of RS. Therefore, others and our results together suggest a portion of SR proteins exist unphosphorylated in the cell so that RS regions can play their roles in RNA binding.

SRSF1 has the shortest RS among the 12 SR proteins. It is likely that RS regions play more important roles in GQ binding for other SR proteins. Among tens of thousands predicted GQ-forming RNA sequences, only a small fraction of them takes GQ conformation in the cell (51). In addition to RNA helicases that unwind RNA GQs, it is inferred that various RNA-binding proteins also prevent GQ formation in the cell (51). However, only a few proteins have been identified to have this function, such as hnRNPH1 (53). The scarcity of proteins binding with G-rich RNA cannot explain how GQ formation is systematically prevented in the cell. Given the abundance of RS-containing proteins, it is likely that SR or SR-like proteins may be one of the main players that prevent GQ formation. Although SRSF1 RRM domains have a secondary role in unfolding GQ, they are important for tight binding to GQ. It is likely that SRSF1 RRMs locate the protein to purine-rich regions for the RS region to unfold the GQ. The RRM domains from other SR proteins may locate the proteins to their cognate RNA motifs and their RS regions unfold neighboring GQ sequences.

We have discovered that interactions between Arg residues in RS regions and the guanine nucleobases play a pivotal role in binding (Figure 4) and unfolding (Figure 5) of ARPC2 GQ. The GQ structure is stabilized by H-bonds, base stacking, and chelation bonds with ions. To unfold GQ, a new set of interactions should be established to replace the interactions stabilizing GQ. The uniqueness of the Arg sidechain lies in its

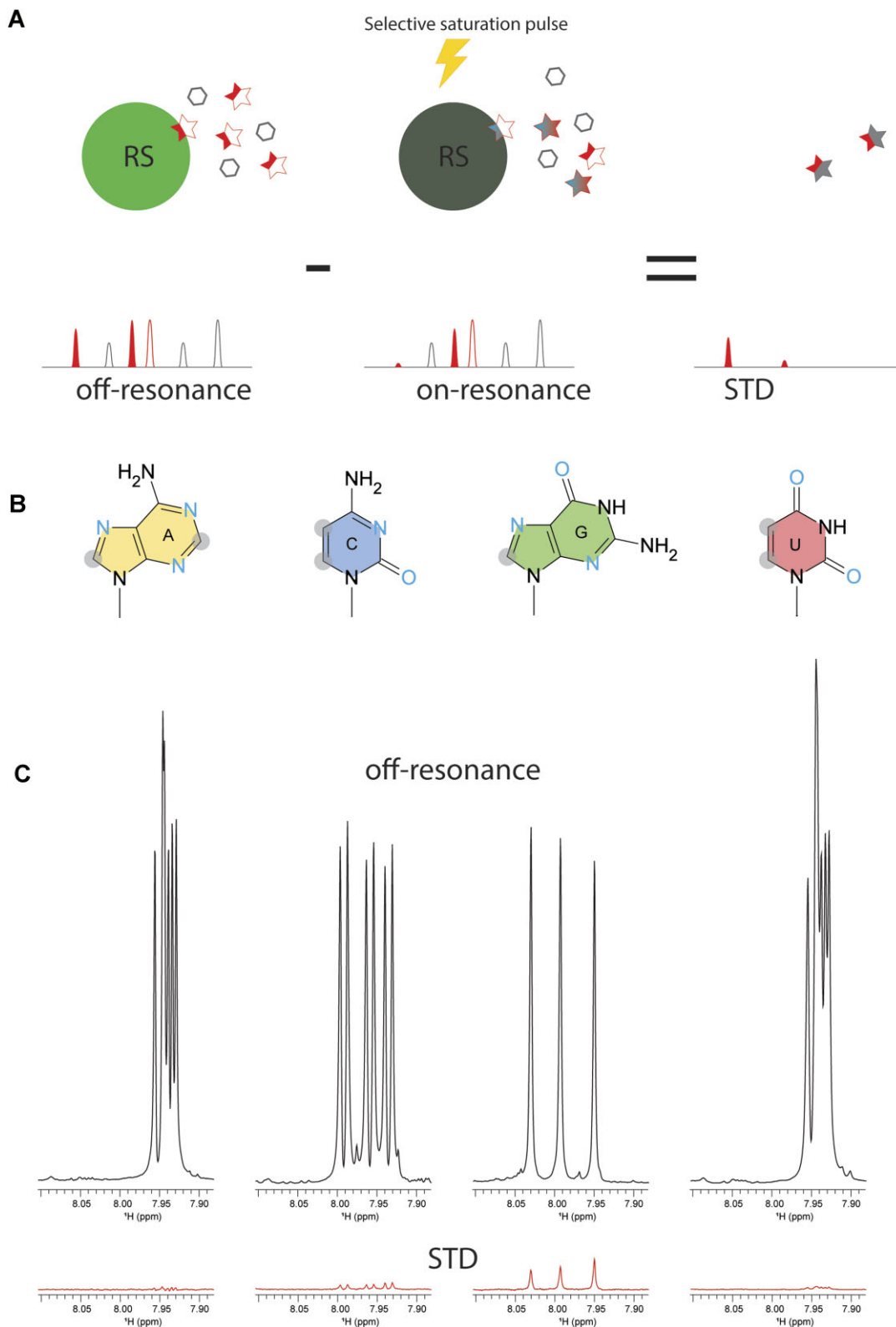


Figure 6. Arg sidechain interacts with guanine. **(A)** Principle of saturation transfer difference (STD) NMR. NMR spectra are collected with and without the saturation pulse focused on the protein region that is away from the ligand resonance. Due to binding and exchange, the NMR signal of the protons directly involved in binding or adjacent to binding sites will be saturated. Subtraction of the saturated spectrum from the unsaturated one yields the STD spectrum, in which only the protons adjacent binding sites survive, and the rest canceled out. **(B)** Structure of nucleobases, with nonexchangeable C–H groups shadowed by gray circle and H-bonding acceptors in blue. **(C)** STD NMR of 3-mer RNA (0.5 mM) with sub-stoichiometry amount of RS (10 μ M). The reference NMR spectra without saturation were shown in black and the STD spectra shown in red. The samples were dissolved in D₂O solution to avoid saturation transfer through solvent. (C) The schematic illustration of interactions between the Arg guanidino group and guanine.

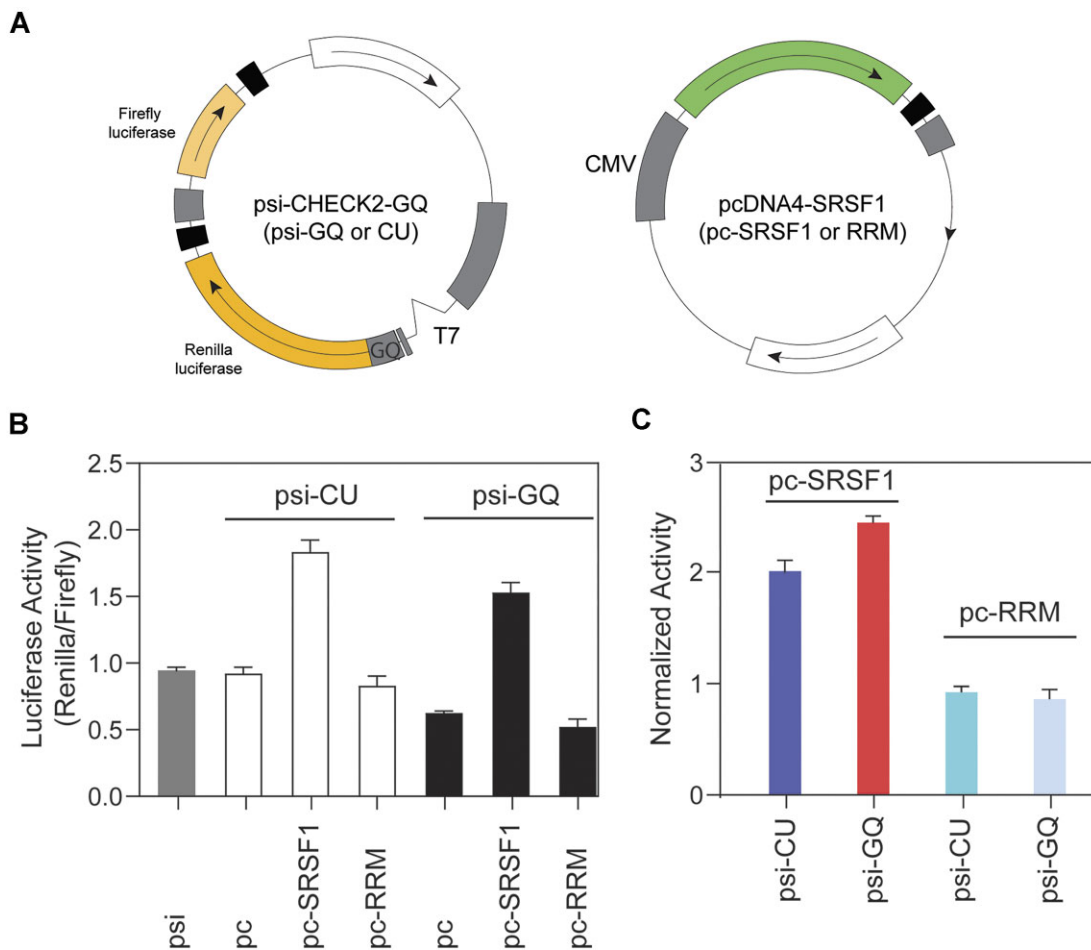


Figure 7. SRSF1 is able to rescue the gene expression inhibited by ARPC2 GQ. **(A)** Plasmid design of psi-CHECK2-GQ or CU. The ARPC2 GQ RNA sequence (21 nucleotides) or CU repeats of the same length was inserted immediately before the starting codon of the Renilla luciferase gene and after the T7 promoter. **(B)** Renilla and firefly luciferase activity ratio for HEK293 cells co-transfected by psi-CHECK2 with ARPC2 GQ (psi-GQ) and empty pcDNA4 (pc) or pcDNA4 encoding SRSF1 (pc-SRSF1) or its RRM tandem (pc-RRM). As a control, co-transfection was also performed for psi-CHECK2 with CU repeats (psi-CU) of the same length as ARPC2 GQ. **(C)** Normalized luciferase activity calculated using the data in panel B. The luciferase activity for pc-SRSF1 or pc-RRM was normalized by the activity of empty pcDNA4 (pc) in each group. For example, the effect of SRSF1 on psi-GQ (red bar in panel C) was calculated by the ratio of pc-SRSF1 to empty pcDNA4 (pc) co-transfected with psi-GQ (panel B).

fork-like sidechain, which can form various interactions with nucleobases, including H-bonds, salt-bridges, and stacking interactions (Figure 8A). Among the four nucleobases, guanine stands out due to its possession of three H-bonding acceptor sites that can form H-bonds with Arg sidechain in multiple ways (Figure 8A). Notably, the Arg sidechain can simultaneously form hydrogen bonds with guanine while creating salt bridges with the phosphate backbone, as visualized in Figure 8B. This dual interaction capability makes Arg/guanine interactions the most prevalent in DNA-binding and RNA-binding proteins according to two comprehensive bioinformatic analyses (59,65). Our STD NMR results have experimentally confirmed that the Arg sidechain specifically interacts with guanine, with no similar interactions observed for other nucleobases. These findings provide a mechanistic foundation for understanding the interactions between RS regions and G-rich sequences. According to our ensemble FRET results, RS-bound ARPC2 GQ takes a more extended conformation than the apo GQ unfolded by thermal denaturation. As thermal denatured polymers assume a random conformation, conformers that have Cy3 and Cy5 close enough

for FRET still exist. However, RS bound ARPC2 GQ has a much lower FRET. This suggests a cooperative binding of SRSF1 RRMs and RS to ARPC2 GQ, which helps maintain the RNA in an extended conformation. It is noteworthy that in this extended conformation, the distance between neighboring backbone phosphates of the RNA ranges from 6.5 to 7.5 Å, closely matching the distance between arginines of the RS dipeptide in the extended conformation (6.8 Å). Based on previous bioinformatics studies and our experimental findings, we propose the model depicted in Figure 8C to elucidate the mechanism by which RS regions unwind GQs. In this model, Arg sidechains form simultaneous H-bonds with guanine bases and salt bridges with phosphate backbones. The number of Arg (19 of them) in the SRSF1 RS exceeds the number of guanines involved in GQ formation. Therefore, enough Arg sidechains are provided to establish these interactions. However, it is noteworthy that interactions between RS and G-rich RNA could be dynamic. As both RS and GQ sequences are repetitive in sequences, relative sliding of the two binding partners enables formation of similar types of interactions. As the number of Arg exceeds the number of guanine

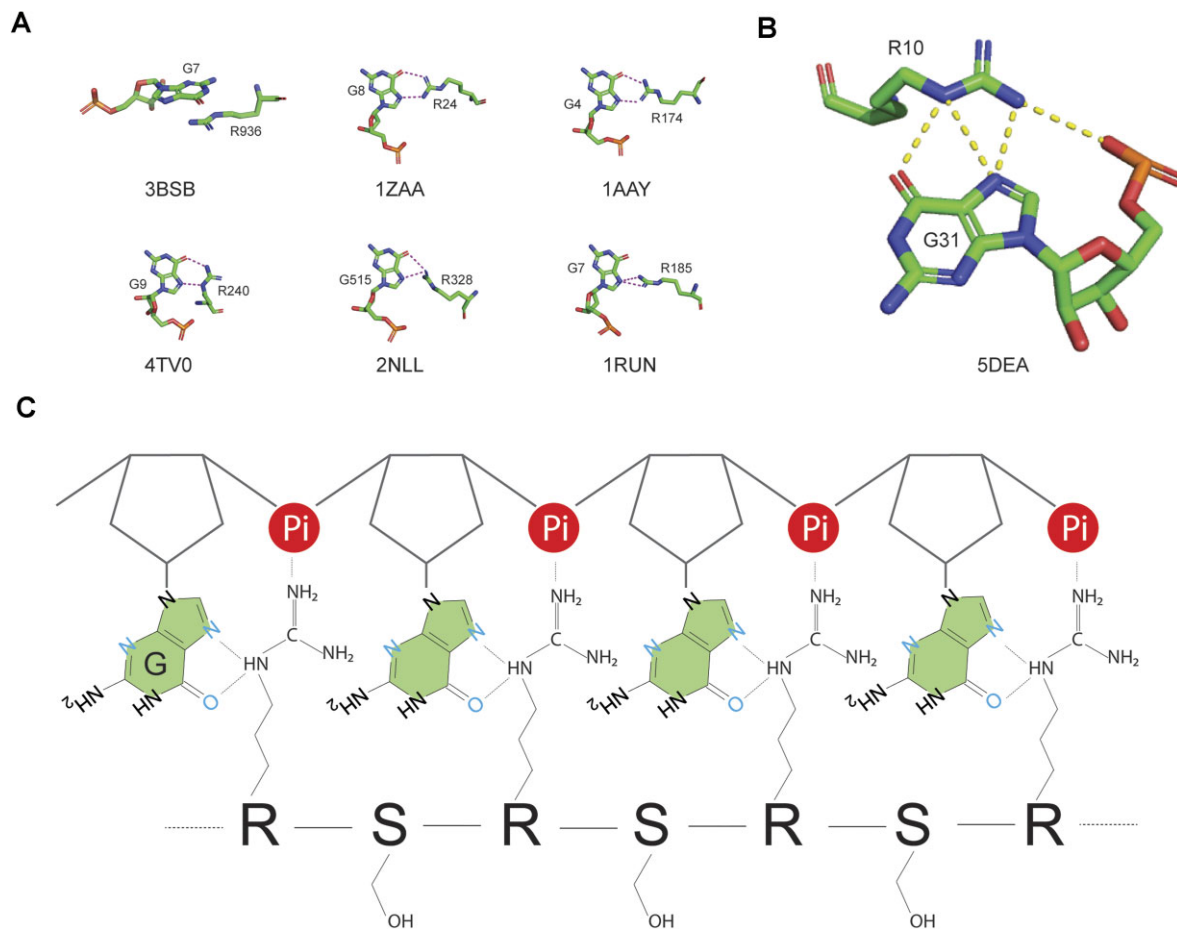


Figure 8. Proposed mechanism by which RS binds unfolded GQ-forming sequences. **(A)** Example stacking interaction or H-bonds between Arg and guanine, with each example accompanied by its residue number and four-letter PDB ID. Dotted lines represent H-bonds. **(B)** A representative interaction is depicted in which the Arg sidechain simultaneously forms H-bonds and a salt bridge with the guanine base and phosphate backbone. **(C)** A schematic representation of the interaction between RS and a G-rich RNA region. In the extended conformation, the distance of neighboring of nucleotides (6.5–7.5 Å) matches that of neighboring the Arg-Ser dipeptide (6.8 Å).

bases in GQs, only a subset of Arg needs to be engaged in dynamic interaction, instead of all Arg forming interactions simultaneously. RS unfolds RNA GQs in a manner distinct from helicases, which unwind RNA GQs in an ATP-dependent way with some of them demonstrating directional processivity (66). The RS binding to guanines shifts the dynamic equilibrium toward the unfolded state.

In a recent genome-wide bioinformatics study, a notable enrichment of GQ sequences has been observed within the exon/intron boundaries (50). It is well-established that these boundaries serve as a critical platform for recruiting numerous splicing factors and spliceosome components. Consequently, it is plausible that the GQ structure represents an additional layer of regulation influencing both constitutive and alternative splicing events. For quite some time, the impact of RNA secondary structure on alternative splicing has been acknowledged, with SR proteins emerging as potential regulators in this context. For example, previous studies have shown that the components of complexes formed around the splicing sites are different depending on whether GQ is formed (67,68). It is inferred that the complexes formed in the presence of GQ is inactive for splicing (68). However, the precise mechanisms governing the collaborative influence of SR proteins and GQ RNA on the splicing process remain a subject that needs further in-depth investigation and exploration.

Data availability

The data underlying this article are available in the article and in its online [Supplementary material](#).

Supplementary data

[Supplementary Data](#) are available at NAR Online.

Acknowledgements

We want to thank UAB Central Alabama High-Field NMR Facility. This work is supported by U.S. National Institutes of Health, NIGMS.

Funding

US National Institutes of Health [R35GM147091-01 to J.Z.]. Funding for open access charge: National Institutes of Health.

Conflicts of interest statement

None declared.

References

- Warf, M.B. and Berglund, J.A. (2010) Role of RNA structure in regulating pre-mRNA splicing. *Trends Biochem. Sci.*, **35**, 169–178.
- Buratti, E. and Baralle, F.E. (2004) Influence of RNA secondary structure on the pre-mRNA splicing process. *Mol. Cell. Biol.*, **24**, 10505–10514.
- McManus, C.J. and Graveley, B.R. (2011) RNA structure and the mechanisms of alternative splicing. *Curr. Opin. Genet. Dev.*, **21**, 373–379.
- van Der Houven Van Oordt, W., Newton, K., Screaton, G.R. and Caceres, J.F. (2000) Role of SR protein modular domains in alternative splicing specificity in vivo. *Nucleic Acids Res.*, **28**, 4822–4831.
- Zahler, A.M., Neugebauer, K.M., Lane, W.S. and Roth, M.B. (1993) Distinct functions of SR proteins in alternative pre-mRNA splicing. *Science*, **260**, 219–222.
- Krainer, A.R., Mayeda, A., Kozak, D. and Binns, G. (1991) Functional expression of cloned human splicing factor SF2: homology to RNA-binding proteins, U1 70K, and Drosophila splicing regulators. *Cell*, **66**, 383–394.
- Ge, H., Zuo, P. and Manley, J.L. (1991) Primary structure of the human splicing factor ASF reveals similarities with Drosophila regulators. *Cell*, **66**, 373–382.
- Fu, X.D. and Maniatis, T. (1990) Factor required for mammalian spliceosome assembly is localized to discrete regions in the nucleus. *Nature*, **343**, 437–441.
- Wahl, M.C., Will, C.L. and Luhrmann, R. (2009) The spliceosome: design principles of a dynamic RNP machine. *Cell*, **136**, 701–718.
- Black, D.L. (2003) Mechanisms of alternative pre-messenger RNA splicing. *Annu. Rev. Biochem.*, **72**, 291–336.
- Wang, E.T., Sandberg, R., Luo, S., Khrebukova, I., Zhang, L., Mayr, C., Kingsmore, S.F., Schroth, G.P. and Burge, C.B. (2008) Alternative isoform regulation in human tissue transcriptomes. *Nature*, **456**, 470–476.
- Pan, Q., Shai, O., Lee, L.J., Frey, B.J. and Blencowe, B.J. (2008) Deep surveying of alternative splicing complexity in the human transcriptome by high-throughput sequencing. *Nat. Genet.*, **40**, 1413–1415.
- Manley, J.L. and Krainer, A.R. (2010) A rational nomenclature for serine/arginine-rich protein splicing factors (SR proteins). *Genes Dev.*, **24**, 1073–1074.
- Zahler, A.M., Lane, W.S., Stolk, J.A. and Roth, M.B. (1992) SR proteins: a conserved family of pre-mRNA splicing factors. *Genes Dev.*, **6**, 837–847.
- Pandit, S., Zhou, Y., Shiu, L., Coutinho-Mansfield, G., Li, H., Qiu, J., Huang, J., Yeo, G.W., Ares, M. Jr and Fu, X.D. (2013) Genome-wide analysis reveals SR protein cooperation and competition in regulated splicing. *Mol. Cell*, **50**, 223–235.
- Li, X. and Manley, J.L. (2005) Inactivation of the SR protein splicing factor ASF/SF2 results in genomic instability. *Cell*, **122**, 365–378.
- Das, R., Yu, J., Zhang, Z., Gygi, M.P., Krainer, A.R., Gygi, S.P. and Reed, R. (2007) SR proteins function in coupling RNAP II transcription to pre-mRNA splicing. *Mol. Cell*, **26**, 867–881.
- Lin, S., Coutinho-Mansfield, G., Wang, D., Pandit, S. and Fu, X.D. (2008) The splicing factor SC35 has an active role in transcriptional elongation. *Nat. Struct. Mol. Biol.*, **15**, 819–826.
- Huang, Y. and Steitz, J.A. (2005) SRprises along a messenger's journey. *Mol. Cell*, **17**, 613–615.
- Sanford, J.R., Gray, N.K., Beckmann, K. and Caceres, J.F. (2004) A novel role for shuttling SR proteins in mRNA translation. *Genes Dev.*, **18**, 755–768.
- Michlewski, G., Sanford, J.R. and Caceres, J.F. (2008) The splicing factor SF2/ASF regulates translation initiation by enhancing phosphorylation of 4E-BP1. *Mol. Cell*, **30**, 179–189.
- Zhang, Z. and Krainer, A.R. (2004) Involvement of SR proteins in mRNA surveillance. *Mol. Cell*, **16**, 597–607.
- Hu, Z.Y., Wang, X.Y., Guo, W.B., Xie, L.Y., Huang, Y.Q., Liu, Y.P., Xiao, L.W., Li, S.N., Zhu, H.F., Li, Z.G., et al. (2016) Long non-coding RNA MALAT1 increases AKAP-9 expression by promoting SRPK1-catalyzed SRSF1 phosphorylation in colorectal cancer cells. *Oncotarget*, **7**, 11733–11743.
- Malakar, P., Shilo, A., Mogilevsky, A., Stein, I., Pikarsky, E., Nevo, Y., Benyamini, H., Elgavish, S., Zong, X., Prasanth, K.V., et al. (2017) Long noncoding RNA MALAT1 promotes hepatocellular carcinoma development by SRSF1 upregulation and mTOR activation. *Cancer Res.*, **77**, 1155–1167.
- Clery, A., Krepl, M., Nguyen, C.K.X., Moursy, A., Jorjani, H., Katsantoni, M., Okoniewski, M., Mittal, N., Zavolan, M., Sponer, J., et al. (2021) Structure of SRSF1 RRM1 bound to RNA reveals an unexpected bimodal mode of interaction and explains its involvement in SMN1 exon7 splicing. *Nat. Commun.*, **12**, 428.
- Clery, A., Sinha, R., Anczukow, O., Corrionero, A., Moursy, A., Daubner, G.M., Valcarcel, J., Krainer, A.R. and Allain, F.H. (2013) Isolated pseudo-RNA-recognition motifs of SR proteins can regulate splicing using a noncanonical mode of RNA recognition. *Proc. Natl. Acad. Sci. U.S.A.*, **110**, E2802–E2811.
- Feng, H., Bao, S., Rahman, M.A., Weyn-Vanhenenryck, S.M., Khan, A., Wong, J., Shah, A., Flynn, E.D., Krainer, A.R. and Zhang, C. (2019) Modeling RNA-binding protein specificity in vivo by precisely registering protein-RNA crosslink sites. *Mol. Cell*, **74**, 1189–1204.
- De Silva, N.I.U., Fargason, T., Zhang, Z., Wang, T. and Zhang, J. (2022) Inter-domain flexibility of human Ser/Arg-rich splicing factor 1 allows variable spacer length in cognate RNA's bipartite motifs. *Biochemistry*, **61**, 2922–2932.
- Zaharias, S., Zhang, Z., Davis, K., Fargason, T., Cashman, D., Yu, T. and Zhang, J. (2021) Intrinsically disordered electronegative clusters improve stability and binding specificity of RNA-binding proteins. *J. Biol. Chem.*, **297**, 100945.
- Maslon, M.M., Heras, S.R., Bellora, N., Eyra, E. and Caceres, J.F. (2014) The translational landscape of the splicing factor SRSF1 and its role in mitosis. *eLife*, **3**, e02028.
- Velazquez-Dones, A., Hagopian, J.C., Ma, C.T., Zhong, X.Y., Zhou, H., Ghosh, G., Fu, X.D. and Adams, J.A. (2005) Mass spectrometric and kinetic analysis of ASF/SF2 phosphorylation by SRPK1 and Clk/Sty. *J. Biol. Chem.*, **280**, 41761–41768.
- Hagopian, J.C., Ma, C.T., Meade, B.R., Albuquerque, C.P., Ngo, J.C., Ghosh, G., Jennings, P.A., Fu, X.D. and Adams, J.A. (2008) Adaptable molecular interactions guide phosphorylation of the SR protein ASF/SF2 by SRPK1. *J. Mol. Biol.*, **382**, 894–909.
- Aubol, B.E., Plocinik, R.M., Hagopian, J.C., Ma, C.T., McGlone, M.L., Bandyopadhyay, R., Fu, X.D. and Adams, J.A. (2013) Partitioning RS domain phosphorylation in an SR protein through the CLK and SRPK protein kinases. *J. Mol. Biol.*, **425**, 2894–2909.
- Lai, M.C. and Tarn, W.Y. (2004) Hypophosphorylated ASF/SF2 binds TAP and is present in messenger ribonucleoproteins. *J. Biol. Chem.*, **279**, 31745–31749.
- Huang, Y., Gattoni, R., Stevenin, J. and Steitz, J.A. (2003) SR splicing factors serve as adapter proteins for TAP-dependent mRNA export. *Mol. Cell*, **11**, 837–843.
- Stojdl, D.F. and Bell, J.C. (1999) SR protein kinases: the splice of life. *Biochem. Cell Biol.*, **77**, 293–298.
- Mermoud, J.E., Cohen, P.T. and Lamond, A.I. (1994) Regulation of mammalian spliceosome assembly by a protein phosphorylation mechanism. *EMBO J.*, **13**, 5679–5688.
- Cho, S., Hoang, A., Sinha, R., Zhong, X.Y., Fu, X.D., Krainer, A.R. and Ghosh, G. (2011) Interaction between the RNA binding domains of Ser-Arg splicing factor 1 and U1-70K snRNP protein determines early spliceosome assembly. *Proc. Natl. Acad. Sci. U.S.A.*, **108**, 8233–8238.
- Blencowe, B.J., Bowman, J.A., McCracken, S. and Rosonina, E. (1999) SR-related proteins and the processing of messenger RNA precursors. *Biochem. Cell Biol.*, **77**, 277–291.
- Boucher, L., Ouzounis, C.A., Enright, A.J. and Blencowe, B.J. (2001) A genome-wide survey of RS domain proteins. *RNA*, **7**, 1693–1701.

41. Kellenberger, E., Stier, G. and Sattler, M. (2002) Induced folding of the U2AF35 RRM upon binding to U2AF65. *FEBS Lett.*, **528**, 171–176.
42. Shen, H. and Green, M.R. (2004) A pathway of sequential arginine-serine-rich domain-splicing signal interactions during mammalian spliceosome assembly. *Mol. Cell*, **16**, 363–373.
43. Shen, H., Kan, J.L. and Green, M.R. (2004) Arginine-serine-rich domains bound at splicing enhancers contact the branchpoint to promote prespliceosome assembly. *Mol. Cell*, **13**, 367–376.
44. Guth, S., Martinez, C., Gaur, R.K. and Valcarcel, J. (1999) Evidence for substrate-specific requirement of the splicing factor U2AF(35) and for its function after polypyrimidine tract recognition by U2AF(65). *Mol. Cell Biol.*, **19**, 8263–8271.
45. Guth, S., Tange, T.O., Kellenberger, E. and Valcarcel, J. (2001) Dual function for U2AF(35) in AG-dependent pre-mRNA splicing. *Mol. Cell Biol.*, **21**, 7673–7681.
46. Shaw, S.D., Chakrabarti, S., Ghosh, G. and Krainer, A.R. (2007) Deletion of the N-terminus of SF2/ASF permits RS-domain-independent pre-mRNA splicing. *PLoS One*, **2**, e854.
47. Cascarina, S.M. and Ross, E.D. (2022) Expansion and functional analysis of the SR-related protein family across the domains of life. *RNA*, **28**, 1298–1314.
48. Ahn, E.Y., DeKelver, R.C., Lo, M.C., Nguyen, T.A., Matsuura, S., Boyapati, A., Pandit, S., Fu, X.D. and Zhang, D.E. (2011) SON controls cell-cycle progression by coordinated regulation of RNA splicing. *Mol. Cell*, **42**, 185–198.
49. Xu, S., Lai, S.K., Sim, D.Y., Ang, W.S.L., Li, H.Y. and Roca, X. (2022) SRRM2 organizes splicing condensates to regulate alternative splicing. *Nucleic Acids Res.*, **50**, 8599–8614.
50. Georgakopoulos-Soares, I., Parada, G.E., Wong, H.Y., Medhi, R., Furlan, G., Munita, R., Miska, E.A., Kwok, C.K. and Hemberg, M. (2022) Alternative splicing modulation by G-quadruplexes. *Nat. Commun.*, **13**, 2404.
51. Guo, J.U. and Bartel, D.P. (2016) RNA G-quadruplexes are globally unfolded in eukaryotic cells and depleted in bacteria. *Science*, **353**, 1382–1382.
52. Fay, M.M., Lyons, S.M. and Ivanov, P. (2017) RNA G-Quadruplexes in Biology: Principles and Molecular Mechanisms. *J. Mol. Biol.*, **429**, 2127–2147.
53. Vo, T., Brownmiller, T., Hall, K., Jones, T.L., Choudhari, S., Grammatikakis, I., Ludwig, K.R. and Caplen, N.J. (2022) HNRNPH1 destabilizes the G-quadruplex structures formed by G-rich RNA sequences that regulate the alternative splicing of an oncogenic fusion transcript. *Nucleic Acids Res.*, **50**, 6474–6496.
54. von Hacht, A., Seifert, O., Menger, M., Schutze, T., Arora, A., Konthur, Z., Neubauer, P., Wagner, A., Weise, C. and Kurreck, J. (2014) Identification and characterization of RNA guanine-quadruplex binding proteins. *Nucleic Acids Res.*, **42**, 6630–6644.
55. Mayer, M. and Meyer, B. (2001) Group epitope mapping by saturation transfer difference NMR to identify segments of a ligand in direct contact with a protein receptor. *J. Am. Chem. Soc.*, **123**, 6108–6117.
56. Mahmood, T. and Yang, P.C. (2012) Western blot: technique, theory, and trouble shooting. *N Am. J. Med. Sci.*, **4**, 429–434.
57. Choi, B.E. and Lee, H.T. (2022) DNA-RNA hybrid G-quadruplex tends to form near the 3' end of telomere overhang. *Biophys. J.*, **121**, 2962–2980.
58. Stein, J.H., Schuller, V., Bohm, P., Tinnefeld, P. and Liedl, T. (2011) Single-molecule FRET ruler based on rigid DNA origami blocks. *ChemPhysChem*, **12**, 689–695.
59. Luscombe, N.M., Laskowski, R.A. and Thornton, J.M. (2001) Amino acid-base interactions: A three-dimensional analysis of protein-DNA interactions at an atomic level. *Nucleic Acids Res.*, **29**, 2860–2874.
60. Zhu, J., Mayeda, A. and Krainer, A.R. (2001) Exon identity established through differential antagonism between exonic splicing silencer-bound hnRNP A1 and enhancer-bound SR proteins. *Mol. Cell*, **8**, 1351–1361.
61. Serikawa, T., Spanos, C., von Hacht, A., Budisa, N., Rappsilber, J. and Kurreck, J. (2018) Comprehensive identification of proteins binding to RNA G-quadruplex motifs in the 5' UTR of tumor-associated mRNAs. *Biochimie*, **144**, 169–184.
62. Cavaloc, Y., Bourgeois, C.F., Kister, L. and Stevenin, J. (1999) The splicing factors 9G8 and SRp20 transactivate splicing through different and specific enhancers. *RNA*, **5**, 468–483.
63. Heinrichs, V. and Baker, B.S. (1995) The Drosophila SR protein RBP1 contributes to the regulation of doublesex alternative splicing by recognizing RBP1 RNA target sequences. *EMBO J.*, **14**, 3987–4000.
64. Anko, M.L., Muller-McNicoll, M., Brandl, H., Curk, T., Gorup, C., Henry, I., Ule, J. and Neugebauer, K.M. (2012) The RNA-binding landscapes of two SR proteins reveal unique functions and binding to diverse RNA classes. *Genome Biol.*, **13**, R17.
65. Chavali, S.S., Cavender, C.E., Mathews, D.H. and Wedekind, J.E. (2020) Arginine Forks Are a Widespread Motif to Recognize Phosphate Backbones and Guanine Nucleobases in the RNA Major Groove. *J. Am. Chem. Soc.*, **142**, 19835–19839.
66. Caterino, M. and Paeschke, K. (2022) Action and function of helicases on RNA G-quadruplexes. *Methods*, **204**, 110–125.
67. Owen, N., Zhou, H., Malygin, A.A., Sangha, J., Smith, L.D., Muntoni, F. and Eperon, I.C. (2011) Design principles for bifunctional targeted oligonucleotide enhancers of splicing. *Nucleic Acids Res.*, **39**, 7194–7208.
68. Smith, L.D., Dickinson, R.L., Lucas, C.M., Cousins, A., Malygin, A.A., Weldon, C., Perrett, A.J., Bottrill, A.R., Searle, M.S., Burley, G.A., *et al.* (2014) A targeted oligonucleotide enhancer of SMN2 exon 7 splicing forms competing quadruplex and protein complexes in functional conditions. *Cell Rep.*, **9**, 193–205.